Supporting Information

Tuning of Single-Molecule Conductance via Regioisomerism and Desilylation in (η^5-Cp)Co(η^4-Cb) Complexes

Ye-Hao Ding,‡,[a] Xin Zuo,‡,[b] Yu-Han Dai,[a] Yuan-Ming Li,[a] Jian-Feng Yan,*,[a] Li-Chuan Chen,*,[b] Dong Xiang,*,[b] and Yao-Feng Yuan*,[a]

([a] Key Laboratory of Molecule Synthesis and Function Discovery, Fujian Province University, College of Chemistry at Fuzhou University, Fuzhou, Fujian, 350108, China. E-mail: yanjianfeng@fzu.edu.cn (Jian-Feng Yan), Yaofeng_yuan@fzu.edu.cn (Yao-Feng Yuan))

([b] Institute of Modern Optics, College of Electronic Information and Optical Engineering, Nankai University, Tianjin 300350, China. E-mail: chen.lichuan@nankai.edu.cn (Li-Chuan Chen), xiangdongde@nankai.edu.cn (Dong Xiang))

(‡ These authors contributed equally to this article.)

Table of Contents

1. Synthetic procedures

1.1 Synthesis of p-Py-TMS and o-Py-TMS

Into a 25 mL three-necked flask equipped with a magnetic stir bar were successively added *n*-decane (5 mL) and **Py-TMS** (550 mg, 3.00 mmol). The mixture was stirred at room temperature for 5 minutes. Subsequently, dicarbonylcyclopentadienylcobalt ($CpCo(CO)_2$) (270 mg, 1.50 mmol, 0.18 mL) was added dropwise, controlling the addition rate to avoid vigorous reaction. The temperature was then raised to 174 °C, and the reaction was allowed to proceed for 4 h, during which the solution color gradually changed from deep reddish-brown to black. After completion, the reaction mixture was cooled to room temperature, filtered through a pad of Celite, and the solvent was removed by rotary evaporation. The crude product was further purified by column chromatography on silica gel (100–200 mesh). Unreacted **Py-TMS** was eluted first using dichloromethane (DCM), followed by collection of the first orange-yellow band using a mixture of ethyl acetate (EA) and DCM (1/10, v/v) as the eluent. The product exhibited an R_f value of 0.48 (EA/DCM, 1/10, v/v). After removal of the solvent by rotary evaporation, a brownish-yellow solid of **p-Py-TMS** was obtained (527 mg, 1.11 mmol), yielding 74% (based on Co). m.p. 191–192 °C. ^{1}H NMR (500 MHz, $CDCl_3$) δ 8.44 (s, 4H, phenyl-H), 7.21 (s, 4H, phenyl-H), 4.86 (s, 5H, Cp-H), 0.16 (s, 18H, -$SiMe_3$). ^{13}C NMR (126 MHz, $CDCl_3$) δ 149.2 (phenyl-C), 147.8 (phenyl-C), 124.0 (phenyl-C), 86.0 (Cb-C), 81.6 (Cb-C), 69.9 (Cp-C), 1.3 (-$SiMe_3$). HRMS (ESI^+) *m/z* Calcd for $C_{25}H_{31}CoN_2Si_2$+H^+ 475.1431 $[M+H]^+$; found 475.1439.

The elution progress was monitored by TLC (EA), R_f = 0.45. The second orange-yellow band was collected using EA as the eluent. After removal of the solvent by rotary evaporation, a brownish-yellow solid of **o-Py-TMS** was obtained (150 mg, 0.32 mmol), yielding 21%(based on Co). m.p. 190–191 °C. ^{1}H NMR (500 MHz, $CDCl_3$) δ 8.41 (s, 4H, phenyl-H), 7.13 (s, 4H, phenyl-H), 4.83 (s, 5H, Cp-H), 0.22 (s, 18H, -$SiMe_3$). ^{13}C NMR (126 MHz, $CDCl_3$) δ 149.0 (phenyl-C), 146.4 (phenyl-C), 123.8 (phenyl-C), 85.0 (Cb-C), 81.7 (Cb-C), 69.1 (Cp-C), 1.8 (-$SiMe_3$). HRMS (ESI^+) *m/z* Calcd for $C_{25}H_{31}CoN_2Si_2$+H^+ 475.1431 $[M+H]^+$; found 475.1431.

1.2 Synthesis of p-Py

To a 100 mL three-necked flask equipped with a magnetic stir bar was added **p-Py-TMS** (200 mg, 0.42 mmol), followed by 10 mL of a 1 M tetrabutylammonium fluoride

(TBAF) solution in THF. The reaction was allowed to proceed at room temperature for 24 h. After removal of the solvent by rotary evaporation, the resulting oily residue was purified by column chromatography on silica gel (100–200 mesh) using a mixture of petroleum ether (PE) and EA (1/1, v/v) as the eluent (R_f = 0.42 in PE/EA, 1/1, v/v). **p-Py** was obtained as a brownish-yellow solid (104 mg, 0.32 mmol) in 75% yield. m.p. 295–296 °C. ^{1}H NMR (500 MHz, $CDCl_3$) δ 8.44 (s, 4H, phenyl-H), 7.07 (s, 4H, phenyl-H), 5.07 (s, 2H, Cb-H), 4.62 (s, 5H, Cp-H). ^{13}C NMR (126 MHz, $CDCl_3$) δ 150.1 (phenyl-C), 147.1 (phenyl-C), 119.4 (phenyl-C), 81.4 (Cp-C), 70.8 (Cb-C), 55.5 (Cb-C). HRMS (ESI$^+$) *m/z* Calcd for $C_{19}H_{15}CoN_2$+H^+ 331.0645 [*M*+H]$^+$; found 331.0640.

1.3 Synthesis of o-Py

o-Py was synthesized following the same procedure as described for **p-Py**. Starting from **o-Py-TMS** (170 mg, 0.36 mmol) and a 1 M TBAF solution in THF (10 mL), a brownish-yellow solid of **o-Py** was obtained (76 mg, 0.23 mmol), corresponding to a 55% yield. m.p. 280–282 °C. ^{1}H NMR (500 MHz, $CDCl_3$) δ 8.53 (s, 4H, phenyl-H), 7.28 (s, 4H, phenyl-H), 4.73 (s, 5H, Cp-H), 4.53 (s, 2H, Cb-H). ^{13}C NMR (126 MHz, $CDCl_3$) δ 150.0 (phenyl-C), 147.4 (phenyl-C), 121.5 (phenyl-C), 81.4 (Cp-C), 72.4 (Cb-C), 58.4 (Cb-C). HRMS (ESI$^+$) *m/z* Calcd for $C_{19}H_{15}CoN_2$+H^+ 331.0645 [*M*+H]$^+$; found 331.0640.

2. NMR characterization

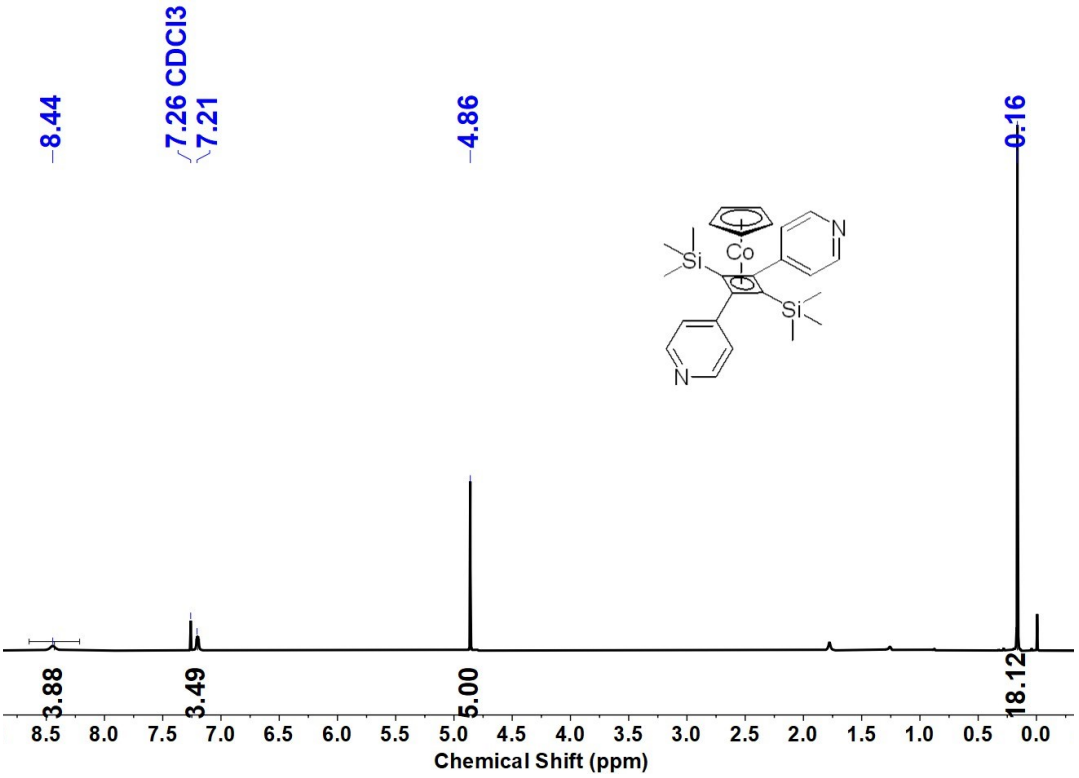

Fig. S1 ^{1}H NMR spectrum of **p-Py-TMS** in $CDCl_3$.

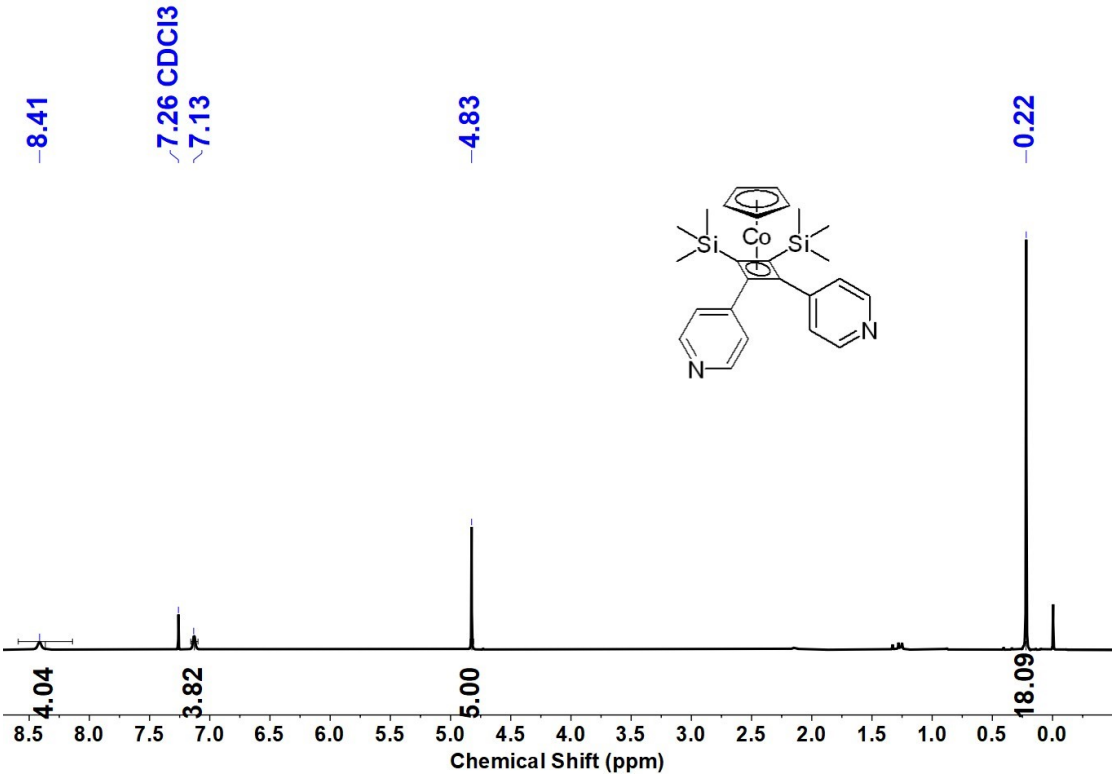

Fig. S2 ^{1}H NMR spectrum of **o-Py-TMS** in $CDCl_3$.

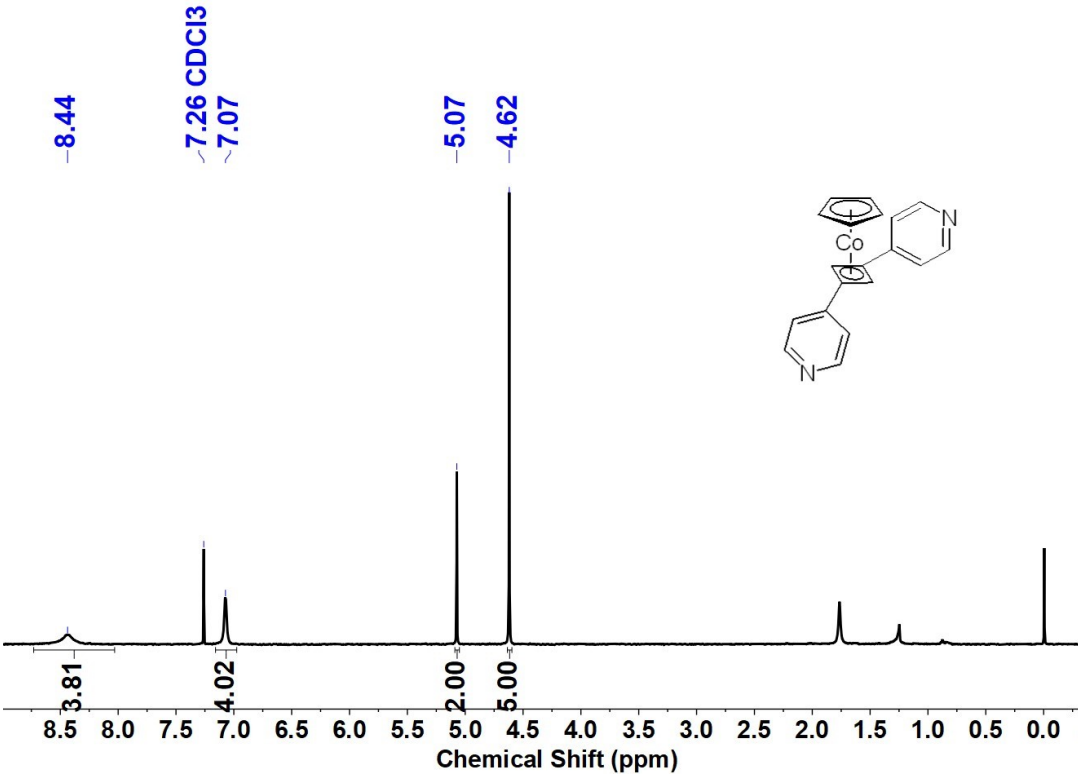

Fig. S3 ^{1}H NMR spectrum of **p-Py** in $CDCl_3$.

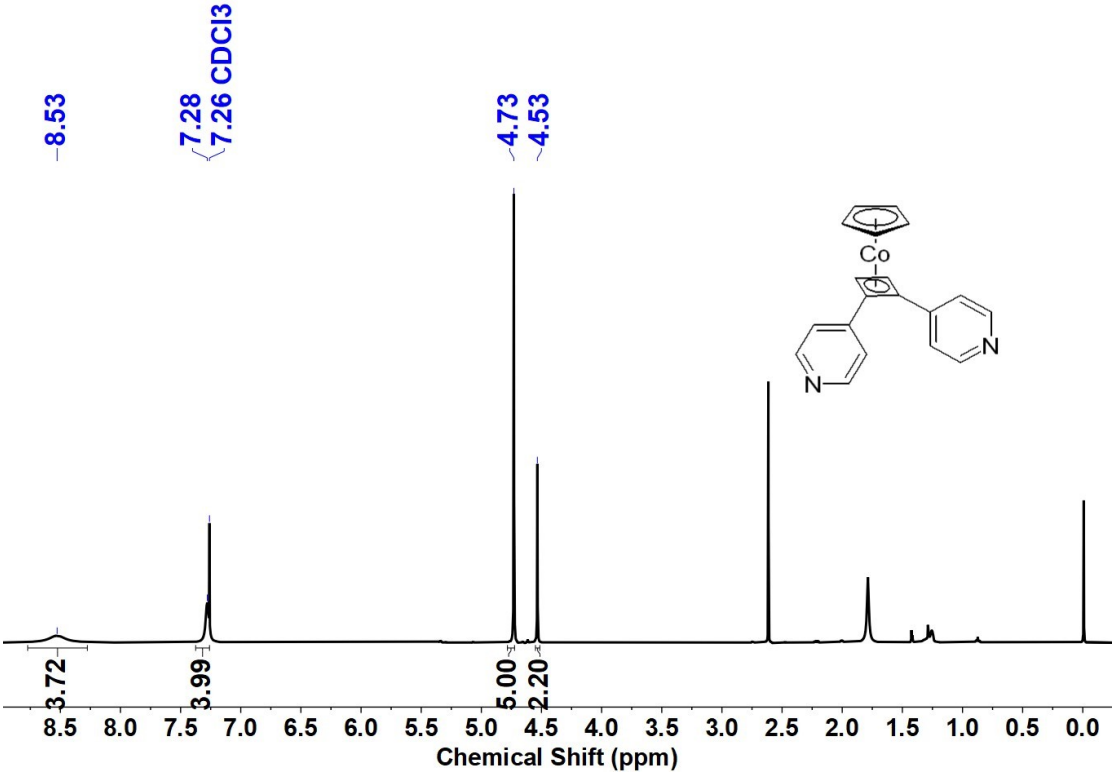

Fig. S4 ^{1}H NMR spectrum of **o-Py** in $CDCl_3$.

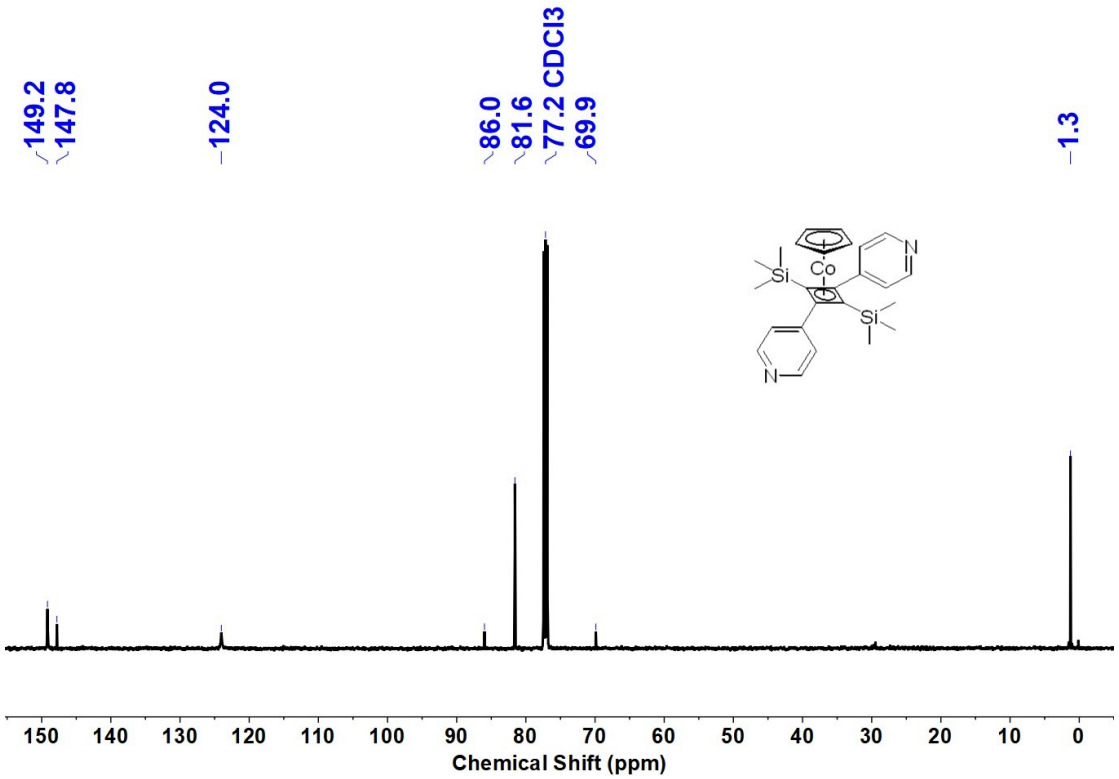

Fig. S5 ^{13}C NMR spectrum of **p-Py-TMS** in $CDCl_3$.

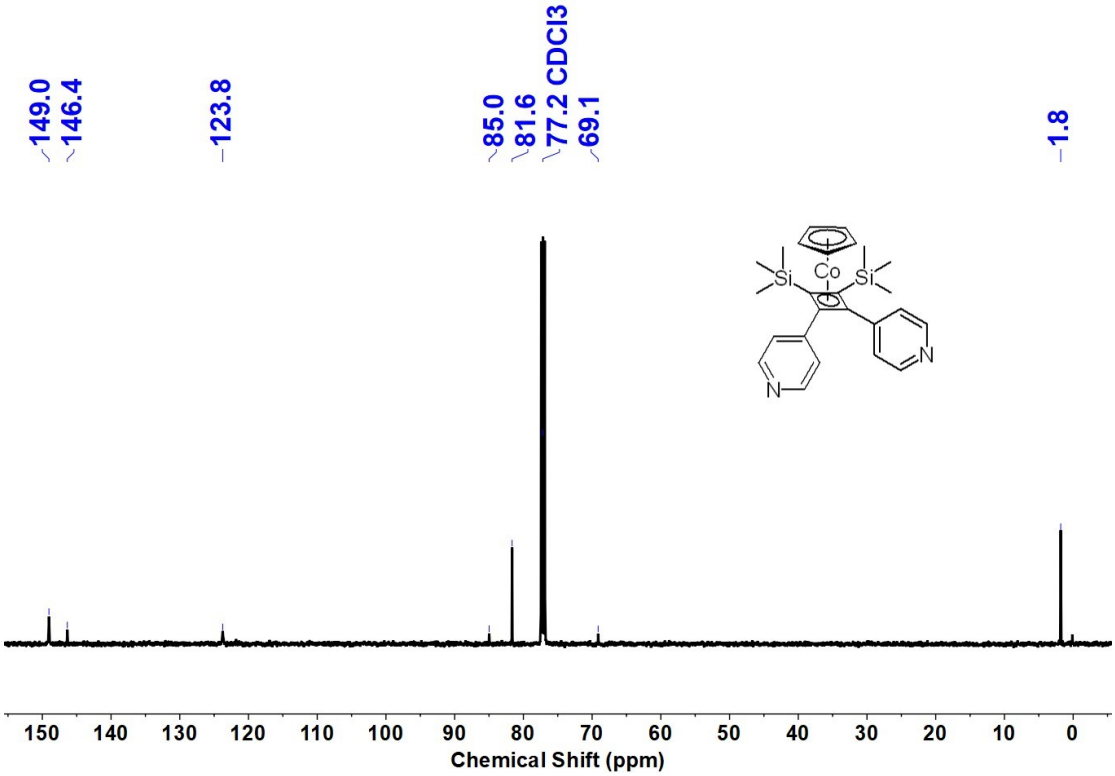

Fig. S6 ^{13}C NMR spectrum of **o-Py-TMS** in $CDCl_3$.

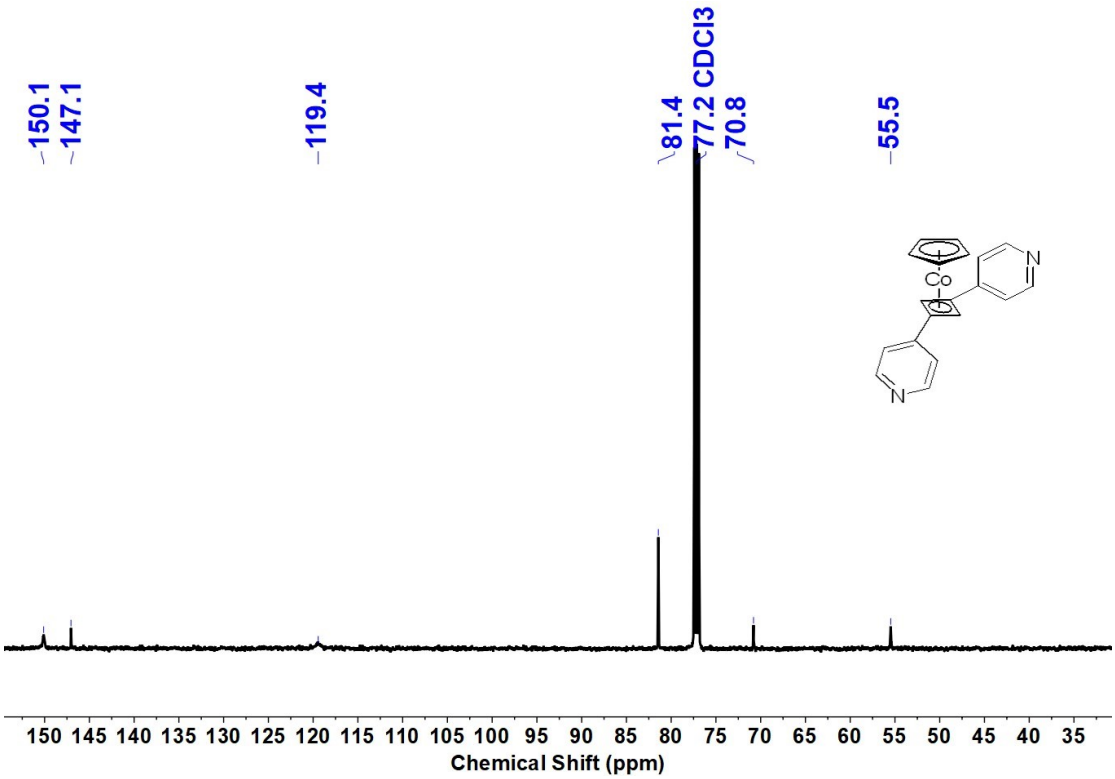

Fig. S7 ^{13}C NMR spectrum of **p-Py** in $CDCl_3$.

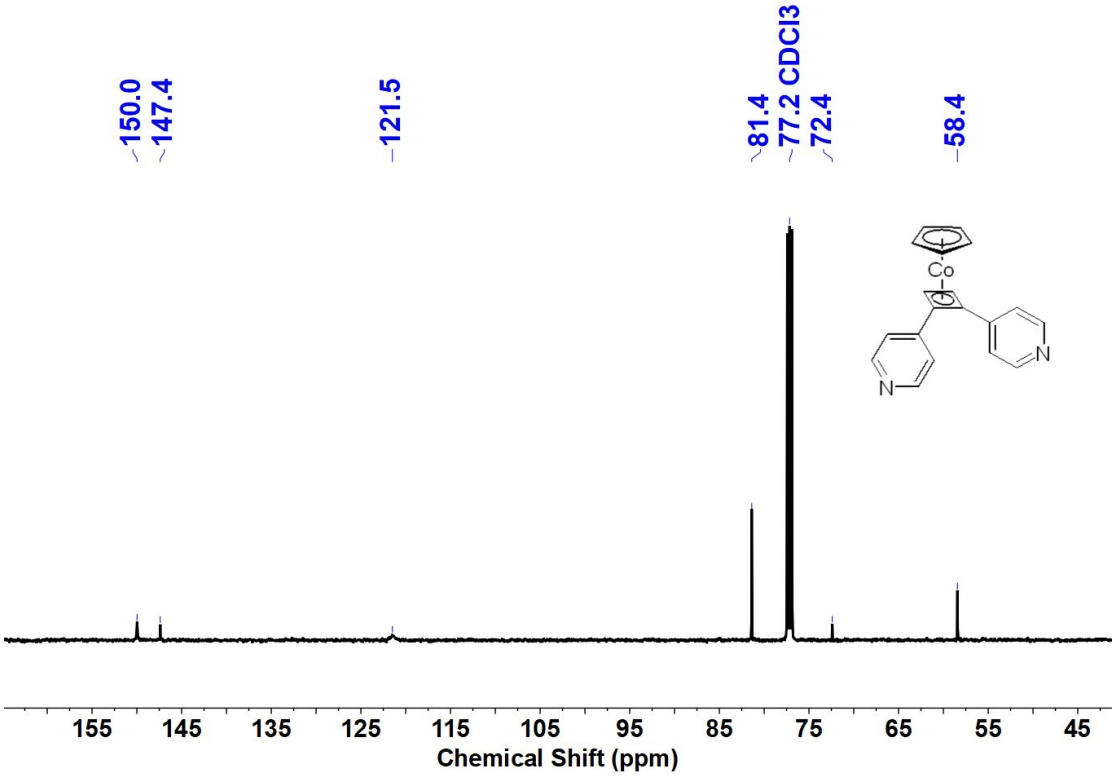

Fig. S8 ^{13}C NMR spectrum of **o-Py** in $CDCl_3$.

3. HRMS characterization

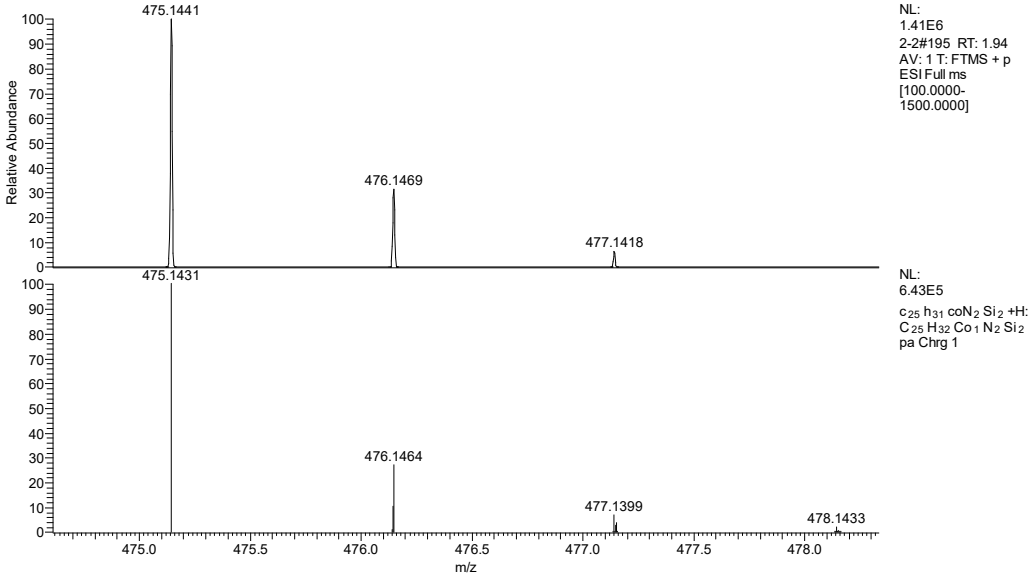

Fig. S9 HRMS of **p-Py-TMS**.

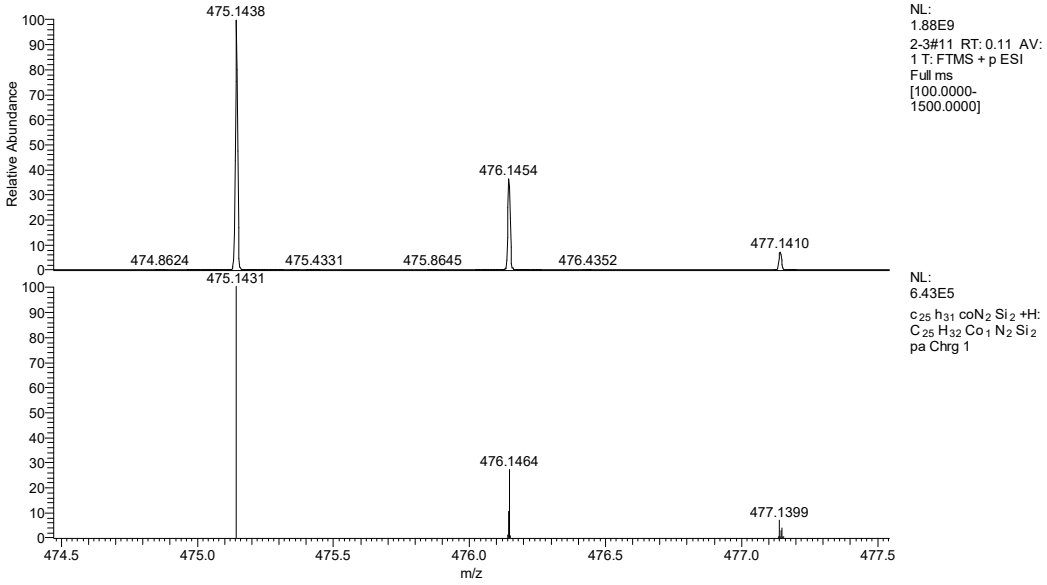

Fig. S10 HRMS of **o-Py-TMS**.

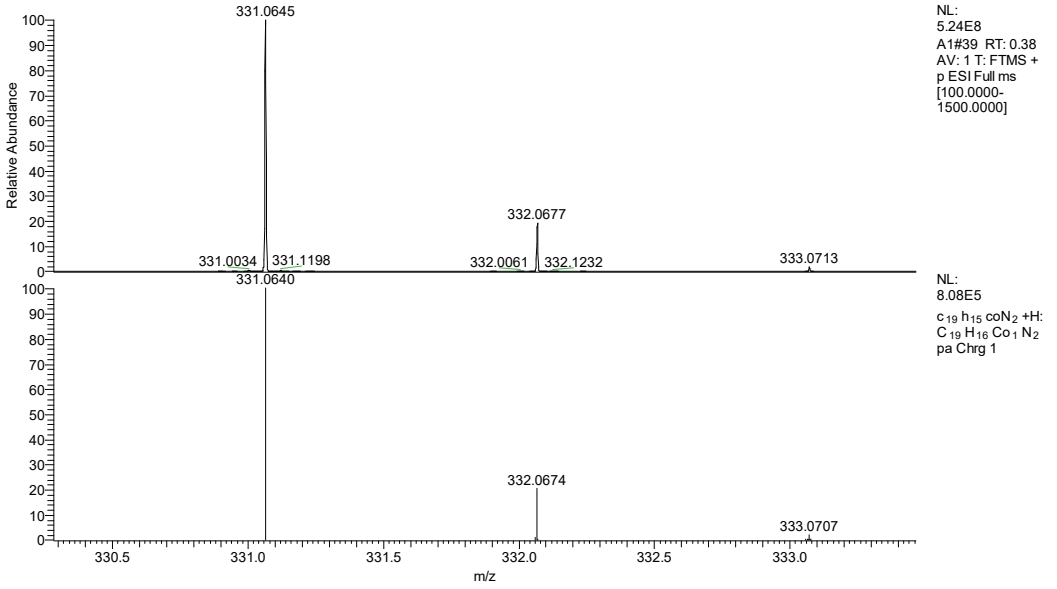

Fig. S11 HRMS of **p-Py**.

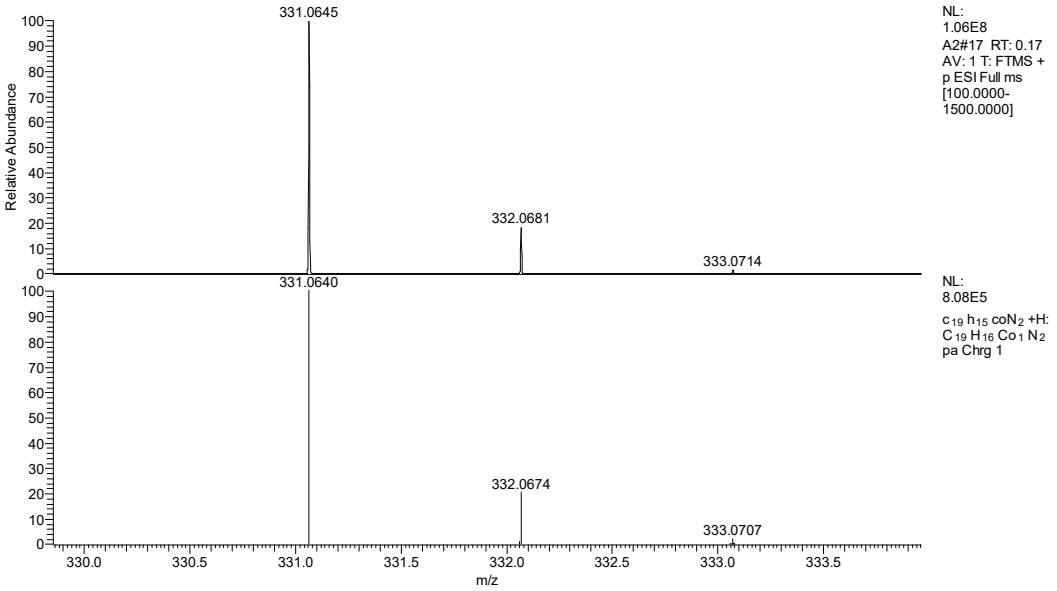

Fig. S12 HRMS of **o-Py**.

4. Crystal data

X-ray diffraction data for the crystals were collected using a Bruker D8 Venture diffractometer. For **p-Py**, data were collected at 296 K using Mo Kα radiation (λ = 0.71073 Å). After data collection, the space group was determined and the structure was solved using direct methods with XPREP from the SHELXTL package.[1] Refinement was performed using Olex2[2] and the SHELX software package[3].

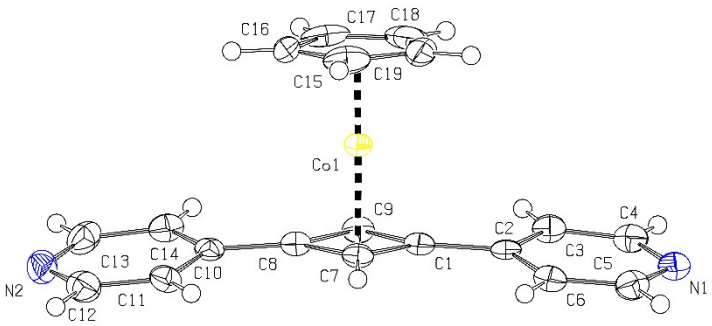

Fig. S13 ORTEP diagram of **p-Py** (drawn at the 50% probability level).

Table S1 Crystallographic data and collection parameters for **p-Py**.

Compound	**p-Py**
CCDC number	2342600
Empirical formula	$C_{19}H_{15}CoN_2$
Formula weight	330.06
Temperature/K	296.15
Crystal system	Orthorhombic
Space group	$Pca2_1$
a/Å	10.3628 (3)
b/Å	19.026 (2)
c/Å	7.5744 (8)
α/°	90
β/°	90
γ/°	90
Volume/Å^3	1493.4 (3)
Z	4
μ/mm^{-1}	1.146
F(000)	680.0
2θ range/°	4.282 to 50.338
Reflections collected	30833
Independent reflections	2674
Data/restraints/parameters	2674/1/199
Goodness-of-fit on F^2	1.021
Final R indices	R_1 = 0.0278 wR_2 = 0.0581
R indices	R_1 = 0.0427 wR_2 = 0.0636

5. Theoretical calculations

5.1 Frontier molecular orbitals

Theoretical calculations were performed using the Gaussian 16 program (Revision C.01),[4] Geometry optimization was conducted at the B3LYP-D3(BJ)/6-31G(d) level of density functional theory (DFT),[5-7]with the SDD pseudopotential basis set applied for cobalt atoms.[8]

Table S2 HOMO–LUMO energy levels of (η^5-Cp)Co(η^4-Cb) derivatives.

Compound	HOMO-1 (eV)	HOMO (eV)	LUMO (eV)	LUMO+1 (eV)	Gap (eV)
o-Py-TMS	–5.92	–5.85	–1.40	–1.32	4.45
o-Py	–5.96	–5.94	–1.52	–1.35	4.42
p-Py-TMS	–6.12	–5.77	–1.44	–0.99	4.33
p-Py	–6.35	–5.66	–1.63	–1.10	4.03

5.2 Comparison of dihedral angles determined from XRD/DFT

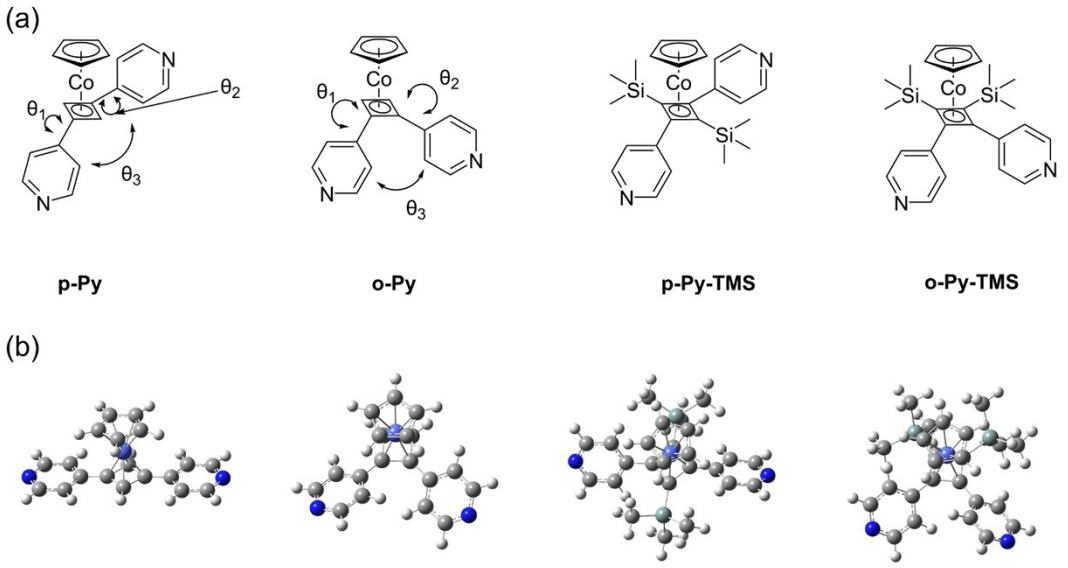

Fig. S14 Molecular structures and dihedral angle definitions for the (η^5-Cp)Co(η^4-Cb) derivatives. Dihedral angles θ_1–θ_3, defined here for **p-Py** and **o-Py,** apply to all four derivatives: θ_1 and θ_2 denote the torsion between pyridine substituents and the core four-membered ring, while θ_3 is the torsion between the two pyridines. (a) Structural diagrams with labeled angles. (b) Geometry-optimized structures.

Table S3 Comparison of XRD and DFT B3LYP-D3(BJ)/6-31G(d) dihedral angles for the rings of (η^5-Cp)Co(η^4-Cb) derivatives and the dominant transport pathway of each compound.

Compound	θ_1 (°)	θ_2 (°)	θ_3 (°)	Dominant pathway
o-Py-TMS (DFT)	35.29	69.37	49.75	through-space
o-Py (DFT)	20.42	27.87	38.84	through-space
p-Py-TMS (DFT)	52.81	36.26	89.06	through-bond
p-Py (DFT)	2.04	2.04	2.00	through-bond
p-Py (XRD)	11.06	10.27	12.83	/

5.3 The NICS(0)$_{zz}$ values, calculated at the geometric center of the core four-membered ring

At the geometric center of the four-membered ring core plane fitted by the least squares method, the relevant calculations were performed using the GIAO method at the B3LYP/6-31+G(d, p) level of theory.[9]

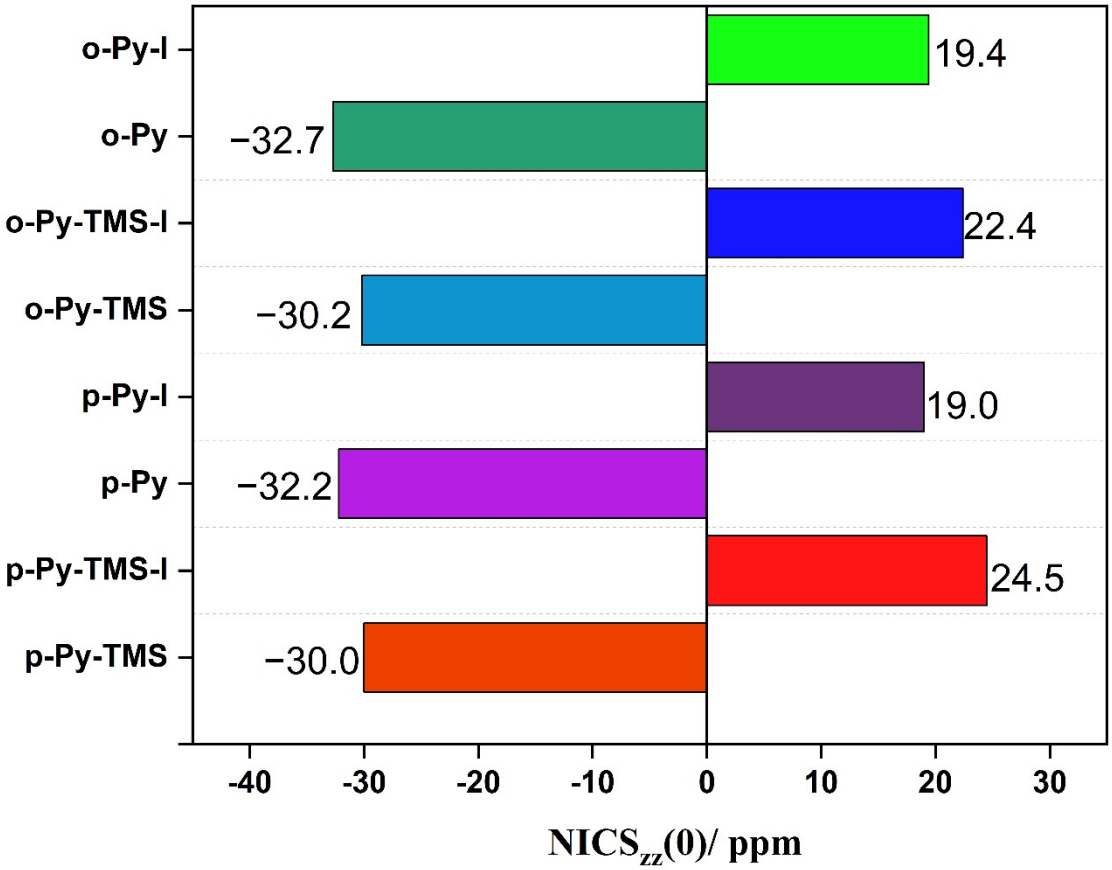

Fig. S15 Comparison of the NICS(0)$_{zz}$ values at the geometric center of the four-membered ring for the series of (η^5-Cp)Co(η^4-Cb) complexes (**p-Py-TMS**, **o-Py-TMS**, **p-Py**, and **o-Py**) and their corresponding free cyclobutadiene ligands (denoted with the suffix "**-l**", e.g., **p-Py-TMS-l**).

5.4 DFT calculation of electron transport through molecular junctions

The optimized structures were further placed between two electrodes to construct single-molecule devices. The surface configuration of the gold electrode was constructed as a pyramid. In the initial configuration of the device, the distance between the N atom and the gold atom of the electrode was controlled at about 2.3 Å. In configuration optimization, the coordinates of all gold atoms in the electrode were fixed and there were no restrictions on the coordinates of the molecules. The geometry optimization and the transmission spectrum of single-molecule junction were performed using the Quantum ATK 2021.06 package.[10, 11] The FHI pseudopotential with a double-ζ basis set was used for Au atoms, and the PseudoDojo pseudopotential with a medium basis set was used for other atoms. A real-space grid with an equivalent energy cutoff of 80 Hartree and the k-points of 3, 3, 134 was used for geometry optimization, and the force threshold is 0.05 eV/Å. In the transmission calculation, transverse k points are increased to 7,7. The Au−N is about 2.2 Å and coplanar with the pyridine ring in the initial configurations of the molecular junctions.

6. Break junction experiments

Prior to STM-BJ experiments, gold substrates were thoroughly cleaned with piranha solution. Gold probe tips were prepared by flame annealing a 0.25 mm diameter gold wire to form smooth gold beads, ensuring a low-noise contact interface. Single-molecule conductance measurements were performed at room temperature using an Xtech STM-BJ 3.0 system (Xiamen Micro-Nano Precision Instruments Co., Ltd.) with 1,2,4-trichlorobenzene as the test solvent and a target molecule concentration of 0.5 mmol L^{-1}. During measurement, a 100 mV DC bias was applied between the gold tip and the gold substrate, and the piezoelectric transducer was driven at a constant rate to achieve periodic contact-breaking cycles, recording conductance-distance curves in real time. All raw data were processed using the open-source software package XMe42 for baseline correction, peak identification, and histogram construction.[12]

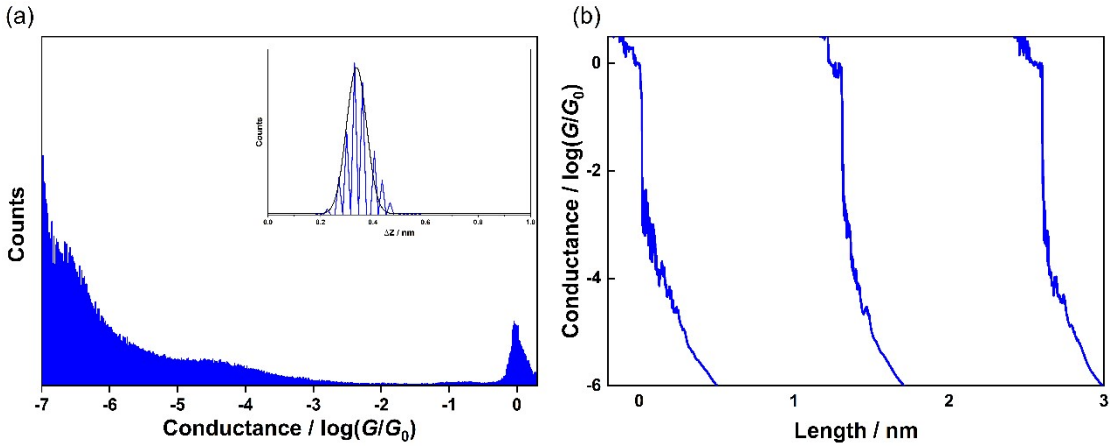

Fig. S16 Characterization during pure solvent correction: (a) one-dimensional conductance histogram with molecular junction length distribution (inset), and (b) a representative single conductance-displacement trace.

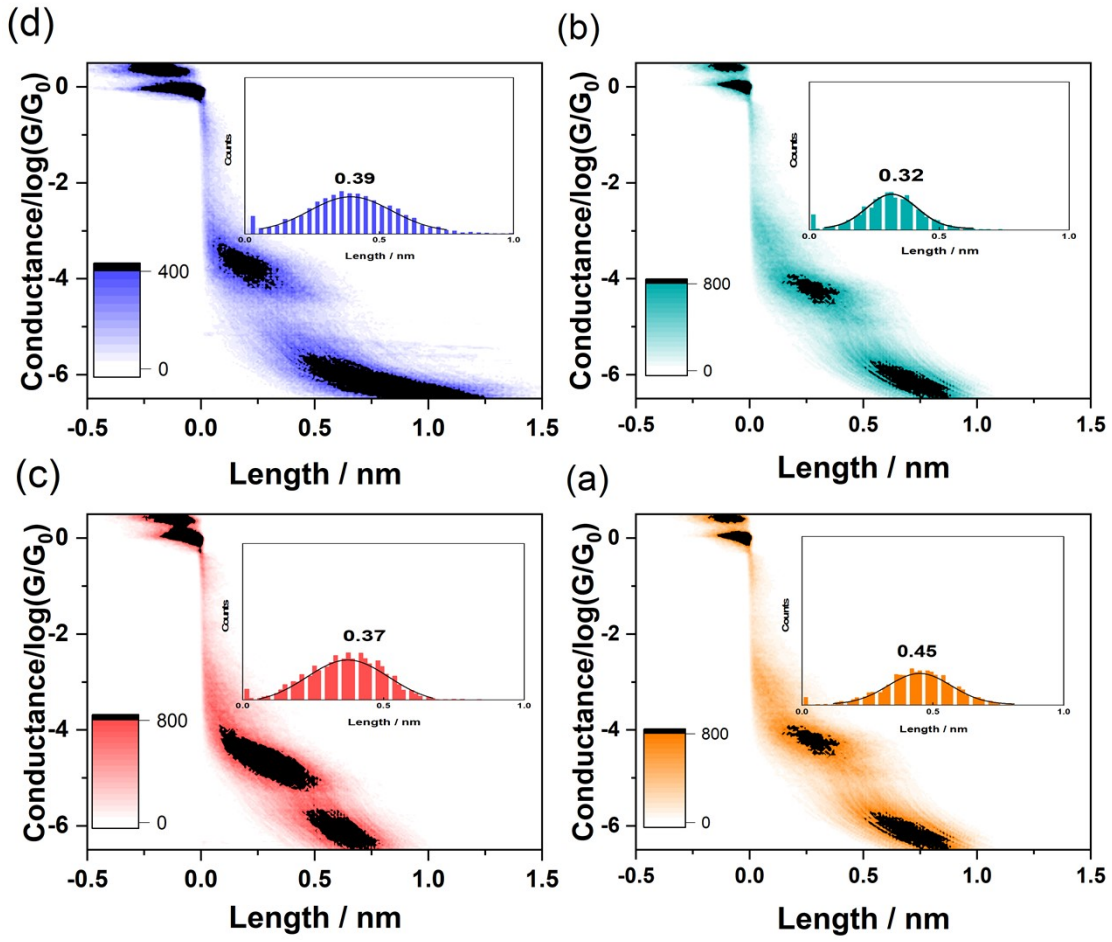

Fig. S17 Two-dimensional (2D) conductance–displacement histograms for (a) **o-Py-TMS**, (b) **o-Py**, (c) **p-Py-TMS**, and (d) **p-Py**. The insets show the corresponding displacement distribution histograms of the single molecular junctions. Conductance peak positions and fitting standard deviations are summarized in Table S4. The N–N distances cited in the main text refer to the intramolecular separation between the two pyridyl nitrogen atoms obtained from DFT-optimized

gas-phase structures. The experimentally measured displacement values reflect the retraction distance of the piezoelectric transducer; after accounting for the snapback of the Au electrodes (typically ~0.5 nm) [13-15], these displacements are consistent with the molecular dimensions expected for the N–N spans of the respective complexes.

Table S4 Single-molecule conductance values and standard deviations obtained from Gaussian fitting of 1D conductance histograms over multiple independent measurements.

Compound	$\log(G/G_0)$ [a]	SD [b]
o-Py-TMS	–3.90	0.05
o-Py	–4.35	0.07
p-Py-TMS	–4.73	0.02
p-Py	–4.28	0.03

[a] Peak conductance values expressed as $\log(G/G_0)$. [b] Standard deviations calculated from $N = 3$ independent experimental batches.

Reference

1. Sheldrick, G.M., *Acta Crystallogr., Sect. A* 1990, ***46*** (6), 467-473.
2. Dolomanov, O., Bourhis, L., Gildea, R., Howard, J., Puschmann, H., *J. Appl. Crystallogr.* 2009, ***42***, 339-341.
3. Sheldrick, G.M., *Acta Crystallogr., Sect. A:Found. Crystallogr.* 2007, ***64*** (1), 112-122.
4. Frisch, M.J., Trucks, G.W., Schlegel, H.B., Scuseria, G.E., Robb, M.A., Cheeseman, J.R., Scalmani, G., Barone, V., Petersson, G.A., Nakatsuji, H., Li, X., Caricato, M., Marenich, A.V., Bloino, J., Janesko, B.G., Gomperts, R., Mennucci, B., Hratchian, H.P., Ortiz, J.V., Izmaylov, A.F., Sonnenberg, J.L., Williams, Ding, F., Lipparini, F., Egidi, F., Goings, J., Peng, B., Petrone, A., Henderson, T., Ranasinghe, D., Zakrzewski, V.G., Gao, J., Rega, N., Zheng, G., Liang, W., Hada, M., Ehara, M., Toyota, K., Fukuda, R., Hasegawa, J., Ishida, M., Nakajima, T., Honda, Y., Kitao, O., Nakai, H., Vreven, T., Throssell, K., Montgomery Jr., J.A., Peralta, J.E., Ogliaro, F., Bearpark, M.J., Heyd, J.J., Brothers, E.N., Kudin, K.N., Staroverov, V.N., Keith, T.A., Kobayashi, R., Normand, J., Raghavachari, K., Rendell, A.P., Burant, J.C., Iyengar, S.S., Tomasi, J., Cossi, M., Millam, J.M., Klene, M., Adamo, C., Cammi, R., Ochterski, J.W., Martin, R.L., Morokuma, K., Farkas, O., Foresman, J.B., Fox, D.J. *Gaussian 16 Rev. C.01*, Wallingford, CT, 2016.
5. Grimme, S., Ehrlich, S., Goerigk, L., *J. Comput. Chem.* 2011, ***32*** (7), 1456-65.
6. Stephens, P.J., Devlin, F.J., Chabalowski, C.F., Frisch, M.J., *J. Phys. Chem.* 1994, ***98*** (45), 11623-11627.
7. Grimme, S., Antony, J., Ehrlich, S., Krieg, H., *J. Phys. Chem.* 2010, ***132*** (15), 154104.
8. Dolg, M., Wedig, U., Stoll, H., Preuss, H., *J. Chem. Phys.* 1987, ***86*** (2), 866-872.
9. Wolinski, K., Hinton, J.F., Pulay, P., *J. Am. Chem. Soc.* 1990, ***112*** (23), 8251-8260.

10. Datta, S., *Electronic Transport in Mesoscopic Systems*. Cambridge University Press: Cambridge, 1995.
11. Brandbyge, M., Mozos, J.-L., Ordejón, P., Taylor, J., Stokbro, K., *Phys. Rev. B* 2002, ***65*** (16), 165401.
12. Pan, Z., Dong, G., Shang, C., Li, R., Gao, T., Lin, L., Duan, H., Li, X., Bai, J., Lai, Y., Wu, W., Shi, J., Liu, J., Hong, W., *Chin. J. Chem.* 2024, ***42*** (3), 317-329.
13. Moreno-García, P., Gulcur, M., Manrique, D.Z., Pope, T., Hong, W., Kaliginedi, V., Huang, C., Batsanov, A.S., Bryce, M.R., Lambert, C., Wandlowski, T., *J. Am. Chem. Soc.* 2013, ***135*** (33), 12228-12240.
14. Kamenetska, M., Koentopp, M., Whalley, A.C., Park, Y.S., Steigerwald, M.L., Nuckolls, C., Hybertsen, M.S., Venkataraman, L., *Phys. Rev. Lett.* 2009, ***102*** (12), 126803.
15. Yanson, A.I., Bollinger, G.R., van den Brom, H.E., Agraït, N., van Ruitenbeek, J.M., *Nature* 1998, ***395*** (6704), 783-785.